AGING ASSESSMENT OF XLPE LV CABLES USED IN NUCLEAR POWER PLANTS

Simone Vincenzo **SURACI**, Chuanyang **LI**, Davide **FABIANI;** DEI – University of Bologna, (Italy), simone.suraci@unibo.it, chuanyang.li@unibo.it, davide.fabiani@unibo.it.

Anne **XU**, Sébastien **ROLAND,** Xavier **COLIN**; PIMM – Arts et Métiers ParisTech, (France), anne.xu@ensam.eu, sebastien.roland@ensam.eu, xavier.colin@ensam.eu

ABSTRACT

This paper investigates the evolution of electrical and physico-chemical properties of low-voltage power cables for nuclear application subjected to both temperature and radiation aging. Electrical response is evaluated by the means of the dielectric spectroscopy technique while the physico-chemical and mechanical changes are analysed at different structural scales by five complementary techniques (FTIR spectroscopy, DSC, OIT, swelling measurement and micro-indentation). All these techniques are shown to be appropriate for the evaluation of the radiochemical aging development on LV cables, suggesting the effectiveness of dielectric spectroscopy as a non-destructive technique for on-site cable diagnosis.

KEYWORDS

XLPE aging, Gamma radiation, nuclear LV cables, low-voltage cables, antioxidant migration, polymer oxidation, dielectric spectroscopy.

INTRODUCTION

Low voltage cables are widely used in nuclear power plants (NPPs) for power transmission, control of equipment and instrumentation, communication (I&C) of signals and data. It has been estimated that inside each NPP there are about 1500 km of cables; since most of the NPPs built during the '80s and '90s are now reaching their end-of-life point, electric utility companies are trying to extend the NPPs operating life up to other 40 years. To do so, low-voltage (LV) I&C cables qualification is a key problem due to the fact that standards set qualification of cables only through destructive techniques [1-2].

As known, the design of nuclear cables can differ depending on the applied voltage and on the specific application (control, power or instrumentation). In any case the most sensitive part in terms of aging is the electrical insulation which surrounds the conductor whose extensive degradation can lead to the failure of the cable. Insulation is made by using polymers which can be filled of different kinds and concentration of additives, above all antioxidants and flame retardants, which can reach very high concentrations (up to 60% w/w) in low voltage power cables.

This research is part of a novel EU Project called "TeaM Cables" which aims at providing NPP operators a novel methodology for efficient and reliable NPP cable ageing management by developing cable aging models and methodologies for non-destructive testing techniques. The materials chosen for analyses inside the TeaM Cables project are the most widely used in power plants:

- Crosslinked Polyethylene (XLPE)
- Ethylene-Vinyl Acetate / Ethylene propylene diene copolymer (EVA-EPDM)

This paper studies the behavior of both electrical and chemical properties with aging on LV power cables made with XLPE insulation. To do so, tests are conducted by the means of both non-destructive (electrical) and standardized destructive techniques (physico-chemical and mechanical). Dielectric spectroscopy technique has been used to analyze the electrical behavior of the insulation and five complementary techniques (FTIR, DSC, OIT, swelling measurement and micro-indentation) have been employed to assess the physico-chemical and mechanical changes. In the end, correlations between these experiments have been carried out.

EXPERIMENTAL SETUP

Specimens

The samples here analysed are low-voltage I&C coaxial cables with XLPE insulation used in NPPs, especially designed for the project. Morphology of the investigated cables is reported in Fig. 1. Specimens are made of five concentric parts:

1. Conductor – Copper (the innermost);
2. Primary insulation – XLPE;
3. Polymeric film;
4. Shielding – Copper wire braid;
5. Outer sheath – Low Smoke Zero Halogen.

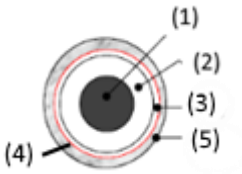

Fig. 1: Morphology of the investigated coaxial cables

The primary insulation, in particular, is a silane crosslinked polyethylene stabilized with 1 phr of primary antioxidant (phenol-based) and 1 phr of secondary antioxidant (thioether-based).

Each cable specimen is about 50 cm long.

Accelerated aging

Aging was performed in the Panoza facility at UJV Rez, Czech Republic. A ^{60}Co γ-ray source was used to fulfil the process. The dose rate set for the aging was 70 Gy/h at 50 °C. Specimens were aged for 200 days and sampling was made about every 40 days. So that, the maximum absorbed dose is 286 kGy.

Electrical measurements

Electrical properties, in particular the complex permittivity, were investigated by means of dielectric spectroscopy technique with a Novocontrol Alpha Dielectric analyser.

The complex permittivity is described as follows:

$$\dot{\varepsilon} = \varepsilon' - j\varepsilon''$$

where: ε' is the real part of permittivity defined as the dielectric constant of the material, and ε'' is the imaginary part of permittivity related to the dielectric losses of the material [1, 3-4].

The instrumentation was set with the following test parameters:

- Applied voltage: 3 V_{rms};
- Frequency range: 10^{-2} – 10^{6} Hz;
- Temperature: 50°C (in oven).

Input voltage was applied to the inner conductor through a BNC plug and output signal was obtained through the copper wire braid shielding.

The device requires, as an input, the reference capacitance in vacuum which was evaluated reducing the cable geometry to a plane capacitor whose diameter was calculated through the following equation:

$$D_{eq} = \sqrt{\frac{d8L}{\ln(R_2/R_1)}}$$

where: *d* is the thickness of the insulation, *L* the length of the metallic mesh, and R_1 and R_2 the inner and outer radius of the electrical insulation respectively.

Finally, the reference capacitance was calculated through:

$$C_o = \varepsilon_0 \frac{\pi\left(\frac{D_{eq}}{2}\right)^2}{d}$$

where: ε_0 is the permittivity in vacuum.

Physico-Chemical measurements

Before any physico-chemical analysis, the cables were stripped from their different successive layers using a specific cutting tool. All physico-chemical measurements were performed exclusively on the XLPE insulation.

Fourier Transform Infrared spectroscopy (FTIR)

FTIR spectroscopy was used to detect the changes in the chemical composition of the insulation during aging (i.e. chemical consumption and migration of antioxidants, and XLPE oxidation). Insulation samples were analysed in an attenuated total reflectance (ATR) mode both on their inner and outer surfaces and in the middle of their cross-section. FTIR spectra were recorded with a Perkin Elmer FTIR Frontier spectrometer equipped with a diamond/ZnSe crystal. Each spectrum corresponds to the average of an accumulation of 16 scans in the spectral range from 4000 to 650 cm^{-1}, with a resolution of 4 cm^{-1}. Any change in absorbance was normalized with the absorbance of CH_2 scissoring vibrations of PE crystal phase at 1472 cm^{-1} [5].

Differential Scanning Calorimetry (DSC)

DSC analysis was used to detect the changes in crystalline morphology of XLPE during aging. Thermograms were recorded with a TA instrument DSC Q1000 calorimeter beforehand calibrated with an indium reference. Insulation samples with a mass ranged between 5 and 8 mg were introduced in a closed standard aluminium pan to be analysed between - 50 °C and 250 °C with heating and cooling rates of 10 °C.min^{-1} and under a pure N_2 flow of 50 mL.min^{-1}. The crystallinity ratio (χ_c) of the polymer was determined as follows:

$$\chi_c = \frac{\Delta H_m}{\Delta H_{m,\infty}}$$

Where ΔH_m and ΔH_∞ are the melting enthalpies (J.g^{-1}) of the sample and PE crystal respectively. In the literature, the commonly used value for ΔH_∞ is 290 J.g^{-1} [6-7].

Oxidation Induction Time (OIT)

DSC analysis was used to monitor the depletion in antioxidants in the bulk of the insulation during aging. Let us remember that OIT is the time required to induce the oxidation reaction of the polymer under a pure O_2 flow at high temperature (typically for T ≥ 190 °C). As the OIT value is near zero at the studied temperatures for the pure XLPE, its measurement gives an assessment of the remaining antioxidant concentration in the radiochemically aged insulation. Thus, when OIT vanishes, all antioxidants are chemically consumed.

OIT was measured at 210 °C with a TA instrument DSC Q10 calorimeter beforehand calibrated with an indium reference. Insulation samples with a mass ranged between 5 and 8 mg were introduced in an opened standard aluminium pan to be submitted to the following program: first of all, heating from room temperature to 210 °C with an heating rate of 10 °C.min^{-1} and under a pure N_2 flow (50 mL.min^{-1}); then, temperature equilibration at 210 °C for 5 min; finally, switching of the gas flow (50 mL.min^{-1}) from N_2 to O_2. The test was considered complete after the entire detection of an exothermal peak corresponding to the polymer oxidation. The OIT value was taken at the onset of the exothermal peak. This onset was determined graphically as the intersection point of the baseline with the steepest tangent of the increasing part of the exothermal peak (i.e. according to the so-called "tangent method").

Swelling measurement

Swelling and extraction in an adequate solvent were used to detect the consequences of XPLE oxidation on its macromolecular network (i.e. chain scissions versus crosslinking). Insulation samples with a mass ranged between 20 and 30 mg (m_i) were weighted with an accuracy of ± 0.01 mg and placed in a round-bottomed flask containing p-xylene (boiling point around 139 °C). This flask was connected to a water-cooled condenser and an adjustable heating mantle so that p-xylene could be heated to reflux. The samples were extracted in refluxing p-xylene for 24h, then they were recovered from the solvent with the help of a funnel and filter paper. The excess solvent on the samples' surface was carefully removed with the help of filter paper, then the samples were quicky transferred into a sealable pre-weighted sample vial and weighted to determine the mass of the swollen gel (m_{sw}). Final drying was carried out in a vacuum chamber at 80 °C up to reach the mass of the dried gel (m_{gel}).

The gel content corresponding to the insoluble fraction (i.e. the proportion of chains participating to the macromolecular network) and swelling ratio can be expressed as:

$$\text{Gel content } (\%) = \frac{m_{gel}}{m_i} \times 100$$

$$\text{Swelling ratio (\%)} = \frac{m_{sw} - m_{gel}}{m_{gel}} \times 100$$

Where m_i, m_{sw} and m_{gel} are the respective masses of the initial sample, swollen gel and dried gel.

Micro-indentation

Micro-indentation was used to detect the consequences of the changes in macromolecular structure and crystalline morphology of XLPE on its elastic properties. As the studied material is the cable insulation, a prior flattening of the surface to be analysed is necessary. Thus, the insulation sample was embedded in a commercial acrylic KM-V resin in order to be polished with a series of abrasive papers of decreasing particle size (typically, from 80 to 2400 granulometry). Indentations were carried out on the outer surface of the insulation with a Micro-Indentation Tester from MSC Instrument equipped with a Vickers-type diamond tip of pyramidal geometry. The force applied was 150 mN, and the loading and unloading rates were 100 $\mu m.min^{-1}$. A pause of 30 s was systematically applied between the loading and unloading.

The indentation operating software gives directly the values of the reduced modulus (E_r) of the material and its Vickers hardness (HV), which are calculated according to the Oliver and Pharr's method [8-9], as follows:

$$E_r = \frac{\sqrt{\pi} S}{2\beta\sqrt{A_c}}$$

$$HV = \frac{2F_{max}}{D^2} * \sin\alpha$$

Where S is the initial slope of the unloading curve, β is a shape factor depending on the indenter type (β = 1.012 for a Vickers tip) and A_c is the contact area between the indenter and sample, which is projected perpendicularly to the indenter axis on the sample surface. A_c is also directly given by the operating software, and depends both on the penetration depth of the indenter and its geometry. α is the opening angle of the Indenter (68°), F_{max} the maximum applied force and D is the measurement of the diagonal of the mark left by the indenter.

The Young's modulus of the sample was then determined from the reduced modulus as follows:

$$E = \frac{1}{\frac{1-\vartheta^2}{E_r} - \frac{1-\vartheta_i^2}{E_i}}$$

Where ϑ is the Poisson's coefficient of the sample ($\vartheta_{Si\text{-}XLPE}$ = 0.42), and ϑ_i and E_i are respectively the Poisson's coefficient and Young's modulus of the diamond indenter (ϑ_i = 0.07 and E_i = 1147 GPa).

RESULTS

Dielectric spectroscopy results

Fig. 2 shows the trend of real and imaginary part of permittivity as a function of frequency for the different aging periods here analysed. As expected, both real and imaginary part of permittivity raise with the increase of aging time.

Referring to Fig. 2.a, the real part of permittivity raises by 0.2 during the first aging period, then it remains almost constant in the further aging periods.

It is noteworthy that the trend of ε' is flat for most of the analysed frequency range except for frequencies lower than 10^{-1} Hz where ε' linearly raises with the decreasing of the applied frequency. This is probably imputed to interfacial phenomena caused by aging, as confirmed by the behaviour of the imaginary part of permittivity (Fig. 2.b). This latter shows an initial decrease in the first aging period with respect to the unaged sample while further aging causes a quite linear increase of ε''. Thus, it is suspected that two physico-chemical mechanisms compete.

Finally, focusing on the lowest frequency range (10^{1}-10^{-2} Hz), the value of the imaginary part of permittivity raises with the decreasing of the frequency. This behaviour is related to an important relaxation peak which occurs at lower frequencies (around 10^{-4} Hz). This peak is linked to interfaces inside the cylindric capacitor measured, as discussed in the following section.

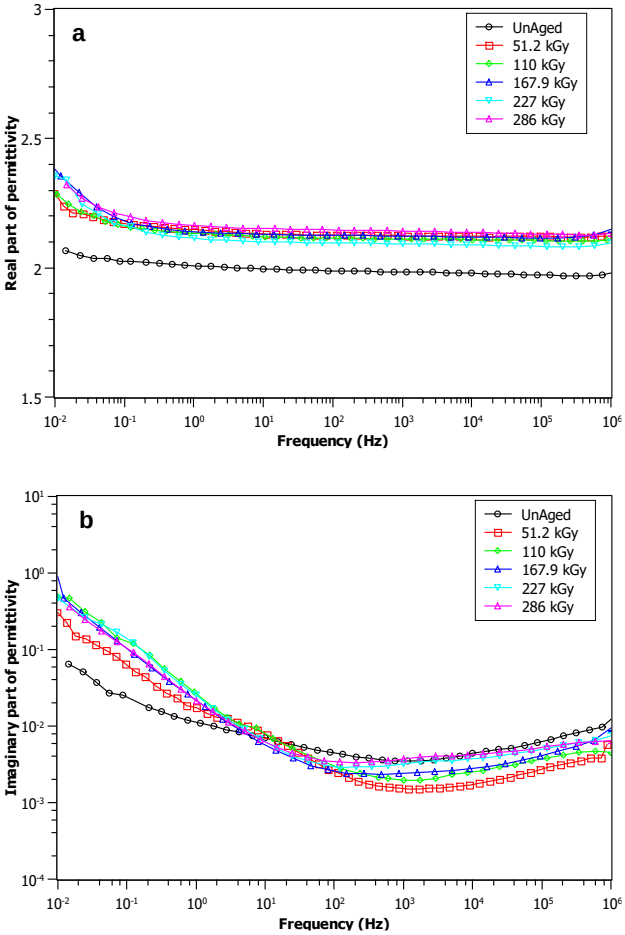

Fig. 2 Dielectric spectra of the real (a) and imaginary (b) part of permittivity as a function of frequency and total dose

Physico-chemical results

OIT measurements

OIT thermograms were measured after different irradiation doses. As an example, in Fig. 3 are given the changes in OIT with aging time. OIT decreases during aging, which is likely due to the chemical consumption of antioxidants by

the stabilization reactions and/or their migration from the bulk to the insulation surface. The drop of OIT is particularly drastic during the first aging period (corresponding to a total irradiation dose of 51.2 kGy), for which OIT is reduced by a factor 6. Then, OIT is still decreasing but less drastically. Finally, it reaches a very low but non-null value (typically 2 minutes) for the highest irradiation dose under study. At 286 kGy, oxidation of XLPE has not started yet.

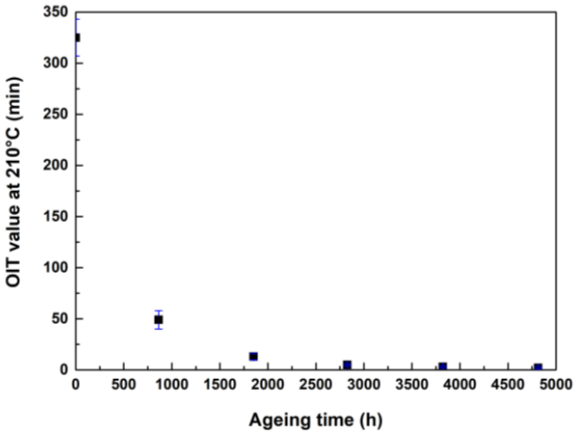

Fig. 3: Changes in OIT with aging time

FTIR spectroscopy

Fig. 4 shows the main changes in the FTIR spectrum of the outer surface of the insulation. These changes occur in three specific spectral regions: (a) between 3500 and 3800 cm^{-1} (hydroxyls), (b) 1600 and 1850 cm^{-1} (carbonyls), and (c) between 900 and 1500 cm^{-1}.

In the carbonyls region, as shown in Fig. 4.b, a single IR peak was observed at 1737 cm^{-1} for the unaged material, attributed to the ester groups of the antioxidants. Then, two new peaks seem to appear during aging in this spectral region: a shoulder at 1720 cm^{-1} and another peak at 1742 cm^{-1}. These two latter peaks seem to increase at the sample surface during aging.

Similarly, in the hydroxyls region (Fig. 4.a), a single small IR peak was observed at 3640 cm^{-1} for the unaged material. This peak is attributed to the phenol function of the phenolic antioxidant. This peak seems to disappear whereas two new small peaks around 3609 and 3580 cm^{-1} seem to appear then decrease during aging.

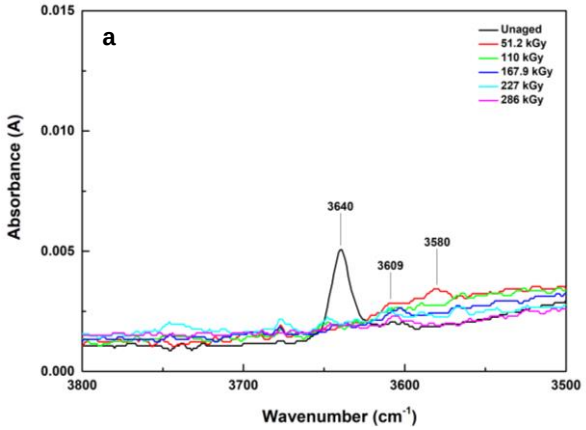

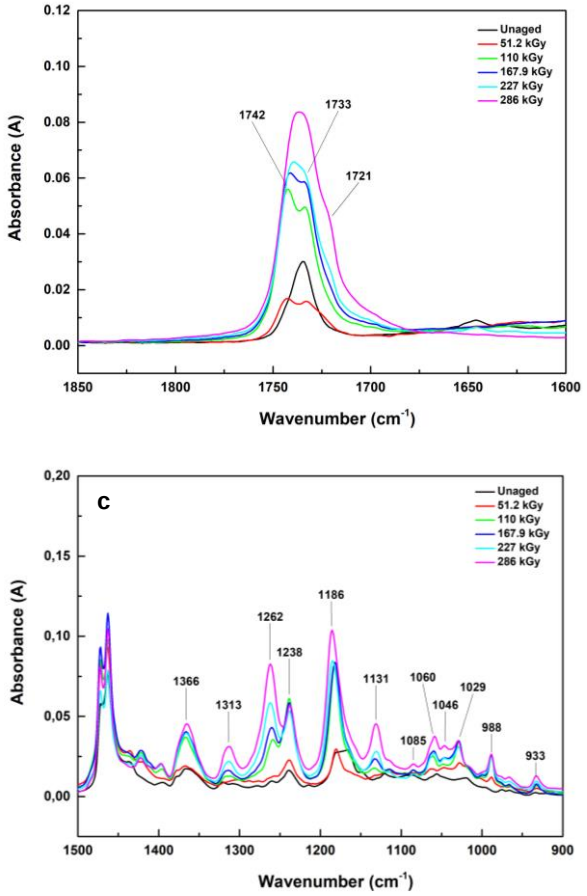

Fig. 4: FTIR spectra of the outer surface of the insulation (a) between 3500 and 3800 cm^{-1}, (b) 1600 and 1850 cm^{-1} and (c) 900 and 1500 cm^{-1}

In the region between 900 and 1500 cm^{-1} (Fig. 4.c), IR peaks at 1366, 1262, 1238, 1186 and 1085 cm^{-1} were initially observed for the unaged sample and are probably due to C-O bonds of ester groups of both antioxidants. These peaks are, as carbonyls peaks, increasing with aging time. Other IR peaks are appearing at 1028, 1046, 1131 and 1313 cm^{-1} during aging, which could be attributed to oxidation products of thioether antioxidants (in particular, sulfoxide and sulfone species) due to stabilization reaction of these antioxidants.

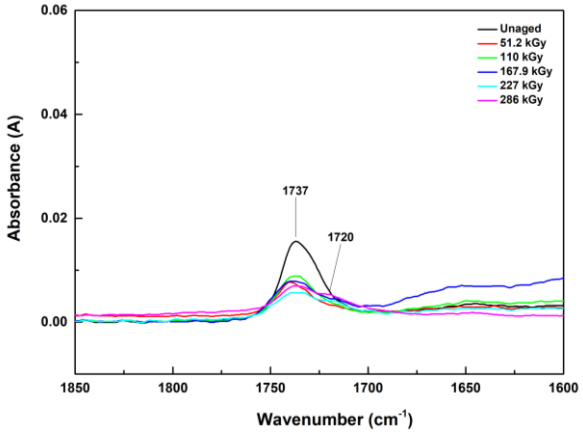

Fig. 5: FTIR spectra of the cross-section of the insulation between 1600 and 1850 cm^{-1}

Fig. 5 shows the changes in the FTIR spectrum of the cross-section of the insulation (exclusively in the carbonyls region). The same observations can be made than previously, that is to say the presence of a single IR peak at 1737 cm^{-1} for the unaged sample. Then, this peak slightly decreases during the first aging duration, then seems to remain almost constant with eventually the appearance of a small shoulder at 1720 cm^{-1} during the rest of aging.

DSC analysis

DSC thermograms were measured after different irradiation doses. As an example, in Fig. 6 are given the changes in cristallinity ratio with aging time. No significant change in cristallinity and melting temperature has occured during aging.

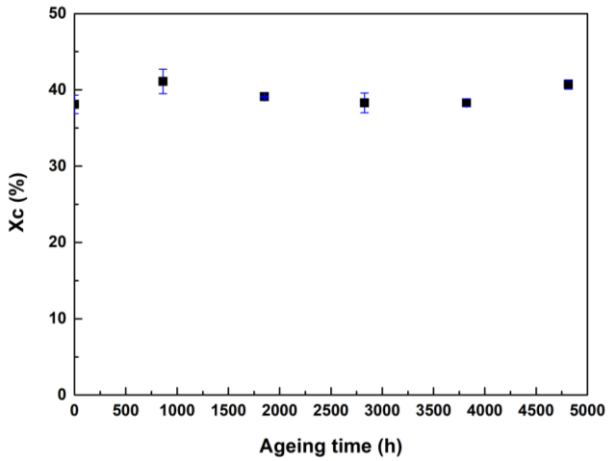

Fig. 6: Changes in cristallinity ratio with aging time

Swelling and gel ratio

In Fig. 7 are given the changes in gel content (a) and swelling ratio (b) with aging time. No significant change in gel content was observed. Concerning swelling ratio, however, a small increase is observed between the second and third irradiation dose, then it remains relatively constant. Therefore, it would seem that a very small number of chain scissions would have occurred, but they have not led to the formation of linear macromolecular fragments yet, but only the formation of dangling chains. This is a typical behavior for very low oxidation ratios, often undetected by conventional spectrochemical methods (such as FTIR) due to their poor sensitivity threshold.

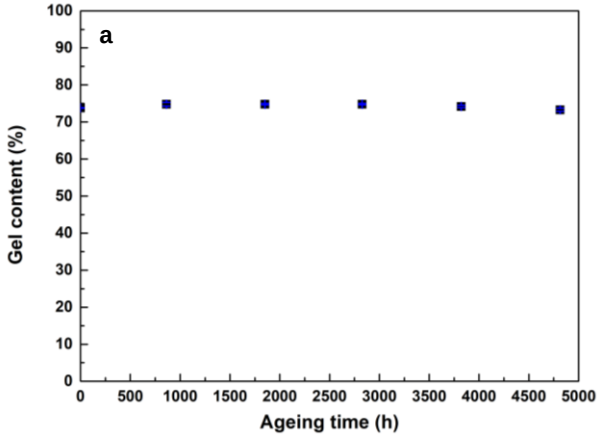

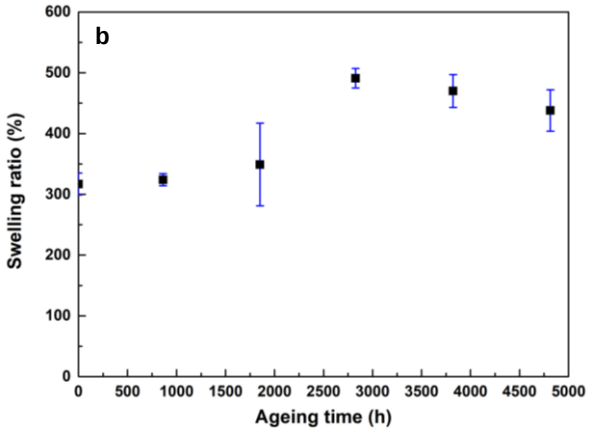

Fig. 7: (a) Changes in gel content and (b) swelling ratio with aging time

Micro-indentation measurement

In Fig. 8 are given the changes in Young's modulus on the outer surface of the insulation with aging time. As for swelling ratio, a small decrease in the Young's modulus is observed between the second and third irradiation dose, after which it remains relatively constant. This small decrease is presumably the result of a small number of chain scissions.

Indeed, it is known that the Young's modulus of an elastomer is related to the concentration of elastically active chains (i.e. molecular chains participating to the network) through the Flory-Rehner theory [10-12]:

$$E = 3\,\nu\rho RT$$

Where E is the Young's modulus, ν the concentration of elastically active chains, ρ the volumic mass of the polymer, R the universal gas constant and T the temperature.

Hence, when chain scissions predominate over crosslinking, the concentration of elastically active chains decreases, causing the decrease of the Young's modulus.

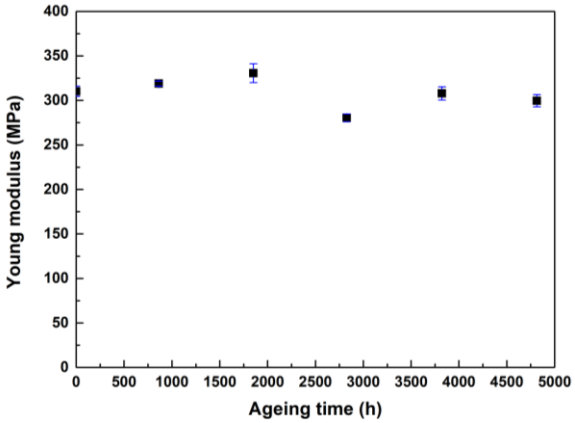

Fig. 8: Changes in Young's modulus with aging time

DISCUSSION

The frequency range investigated through the dielectric spectroscopy technique is referred to both lower frequencies dipolar polarization (10^6 – 10^2 Hz) and

interfacial polarization (lower than 10^2 Hz).

As reported in literature [4], the highest frequency range analysed is related to the polarization of large dipolar species. These ones, e.g. oxidized polymer groups, are often created through the action of aging factors like e.g. high temperatures and radiation, which catalyse oxidative reactions mainly responsible for the degradation of polymers [4]. For this reason, the high frequency range of the imaginary part of permittivity has been shown in previous works [3, 13-14] to be associated with the growth of oxidative products in the polymer matrix during aging.

Nevertheless, it is worth commenting that, for cables here investigated, aging conditions do not yield to a significant oxidation of the primary insulation as shown by the physico-chemical analysis. Indeed, as it can be seen on Fig. 3, OIT decreases with ageing but still remains non-null, meaning that antioxidants are still present and protect the cable insulation against oxidation. Crystallinity ratio and gel content also do not display significant variation during aging (as it can be shown in Fig.6 and Fig. 7.a), meaning that very small changes in the macromolecular network and crystalline morphology of XLPE have occurred.

The drastic decreasing of the imaginary part of permittivity observed during the first aging period (Fig. 1.b) could be due to the chemical consumption of antioxidants. Indeed, OIT decreases drastically during this first period (Fig. 3) while the active functions of phenolic antioxidants disappear (at 3640 cm^{-1}) and those of thioester antioxidants are converted into sulfoxide and sulfone functions (at 1028, 1046, 1131 and 1313 cm^{-1}) (Fig. 4).

Then, FTIR also highlighted the migration of antioxidants from the bulk to the insulation surface with the appearance of new ester (at 1720 and 1742 cm^{-1}) and phenol peaks (at 3580 and 3609 cm^{-1}). In Fig. 9 have been plotted given the changes in ester index (absorbance ratio between all ester peaks and the reference peak at 1472 cm^{-1}) with aging time in the bulk and on the outer surface of the insulation. The ester index quickly increases with aging time on the outer surface, especially from the second aging duration, while it seems to slightly decrease in the bulk. These new peaks could be attributed to different crystalline structures of antioxidants formed on the insulation surface. This phenomenon called polymorphism have already been observed in literature for several phenol antioxidants [15].

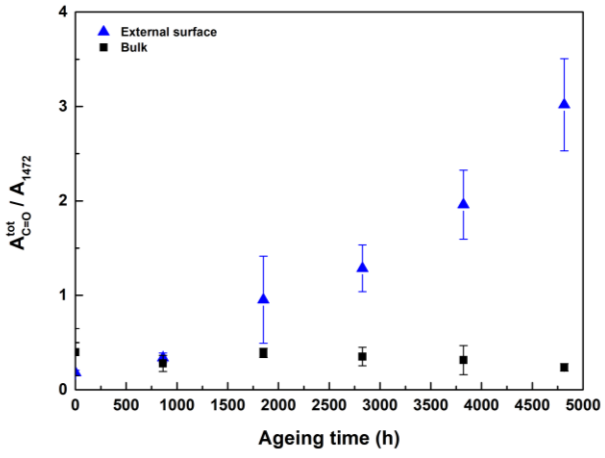

Fig. 9: Changes in the ester index with aging time in the bulk and on the outer surface of the insulation

The accumulation of antioxidants on the outer surface of the insulation could create a thin layer exhibiting a higher electrical conductivity than the primary insulation which can give rise to the high frequency electrical response.
Indeed, the AOs molecules, which made up the layer on the outer insulation surface, can act as induced dipoles following the applied alternating electric field even at high frequencies, similarly to ionic polarization which may occur in crystals causing the raise of dielectric losses in the high frequency region (Fig. 2.a).
Moreover, the longer is the aging period the higher is the increase of AOs molecules on the outer surface (as reported in Fig.7). The accumulation of these highly dipolar species may affect the highest frequency range dielectric response, raising the value of ε'' as reported in Fig. 2.b.

Fig. 10 shows the imaginary part of permittivity at 100 kHz plotted as a function of the total absorbed dose.
As presented, the value of ε'' shows an abrupt reduction imputable to the huge antioxidants consumption as confirmed by the OIT measurements (Fig. 3.b). The regression line showed in Fig. 10 (built from the first aging period on) well fits with the total dose absorbed by the specimens during aging.
This behaviour confirms the strict correlation between evolution of aging and, contextually, its products (above all dipolar species), and the imaginary part of permittivity at 10^5 Hz. Therefore, ε'' at 100 kHz may be also used as an indicator for development of dielectric properties of the material with aging other than a marker for aging state of the insulation.

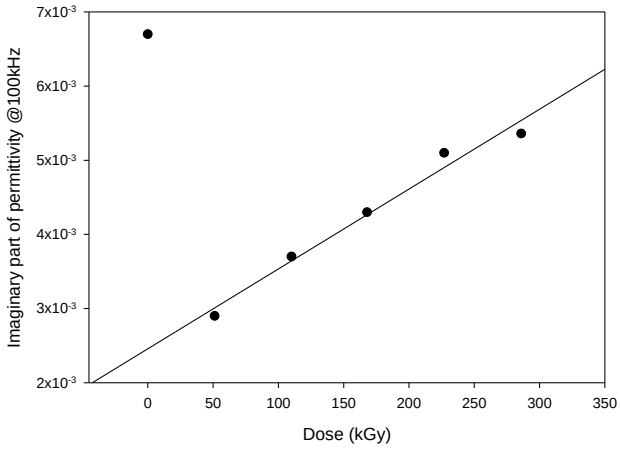

Fig. 10: The imaginary part of permittivity at 100 kHz plotted as a function of total dose.

The interfacial polarization is usually known as Maxwell-Wagner-Sillars polarization [4]. This is caused by the limited diffusion of space charges inside the dielectric by the means of the applied electric field. These charges may settle next to interfaces or discontinuities inside the dielectric itself.
These interfaces can be both physical (interfaces between different materials) and chemical (interfaces between crystalline, amorphous phase and fillers).
In this case, from the morphology of the cable sample it is known that during the extruding process, in order to facilitate the procedure, a polymeric film is placed between the primary insulation (XLPE) and the external copper braid. Due to the experimental setup used, analyses include this film whose interface between the copper braid and the insulation is prone to charge accumulation. This

gives rise to the polarization peak just discussed, appearing for the whole set of specimens considered (unaged and aged ones).
Furthermore, this peak increases with aging, suggesting that this latter leads to the creation of new interfaces which are not only physical, but created during aging inside the primary insulation.
This interface polarization may be related to the conductive AO layer abovementioned other than the presence of ionic and radical species created during the aging process, which can migrate because of the electric field applied and may collect near the interfaces.

CONCLUSIONS

This paper investigated the evolution with aging of electrical and physical-chemical properties of LV XLPE insulated cables for nuclear application.

Cable aging has been monitored through six different measurements techniques, allowing a spread characterization of the analysed XLPE insulation.
In particular, the development of physical-chemical properties has been correlated to the increase of the ε'', and contextually of the dielectric losses, in the highest frequency range with aging.

It has been shown that aging caused an important chemical consumption of antioxidants (showed by OIT measurements) leading to an abrupt decrease of the imaginary part of permittivity (Fig. 2.b) during the first aging period. Further aging has yielded to the migration of antioxidants molecules from the inner part of the insulation to the surface (as showed by the ester index in Fig. 9). These molecules, as highly conductive, caused the raise of the imaginary part of permittivity with aging.
In conclusion, it has been presented that the imaginary part of permittivity, and in general the dielectric losses, can be linked to the change of antioxidants morphology and arrangement in addition to the evolution of aging.

Further research will include the evolution of additional macroscopical mechanical properties (e.g. elongation-at-break) and other electrical measurements (e.g. conductivity tests) in order to obtain a complete outlook of the variation of properties with aging from the micro to the macro scale.

ACKNOWLEDGMENTS

The project leading to this application has received funding from the Euratom research and training programme 2014-2018 under grant agreement No 755183

REFERENCES

[1] L. Verardi, "Aging of nuclear power plant cables: in search of non-destructive diagnostic quantities", PhD Thesis, University of Bologna, 2014.
[2] International Atomic Energy Agency, "Management of life cycle and ageing at nuclear power plants – Improved I&C maintenance", 2004.
[3] E. Linde, L. Verardi, D. Fabiani, U.W. Gedde, "Dielectric spectroscopy as a condition monitoring technique for cable insulation based on crosslinked polyethylene", Polymer testing, 2015, 44.
[4] J.D. Menczel, R.B. Prime, "Thermal analysis of polymers", Wiley, 2009.
[5] P. Pagès, *Characterization of polymer materials using FT-IR and DSC techniques*. Universidade da Coruña, 2005.
[6] Bensason S., Minick J., Moet A., Chum S., Hiltner A., and Baer E., "Classification of homogeneous ethylene-octene copolymers based on comonomer content," *Journal of Polymer Science Part B: Polymer Physics*, vol. 34, no. 7, pp. 1301–1315, Dec. 1998.
[7] K. Sirisinha and S. Chimdist, "Comparison of techniques for determining crosslinking in silane-water crosslinked materials," *Polymer Testing*, vol. 25, no. 4, pp. 518–526, Jun. 2006.
[8] T. Iqbal, B. J. Briscoe, and P. F. Luckham, "Surface Plasticization of Poly(ether ether ketone)," *European Polymer Journal*, vol. 47, no. 12, pp. 2244–2258, Dec. 2011.
[9] E. Courvoisier, Y. Bicaba, and X. Colin, "Multi-scale and multi-technical analysis of the thermal degradation of poly(ether imide)," *Polymer Degradation and Stability*, vol. 147, pp. 177–186, Jan. 2018.
[10] P. J. Flory, *Principles of Polymer Chemistry*. Cornell University Press, 1953.
[11] J. VERDU and X. COLIN, "Structures macromoléculaires tridimensionnelles," *Ref : TIP100WEB - "Plastiques et composites,"* 10-Jan-2008. [Online]. Available: https://www.techniques-ingenieur.fr/base-documentaire/materiaux-th11/plastochimie-et-analyse-physico-chimique-42139210/structures-macromoleculaires-tridimensionnelles-am3045/. [Accessed: 29-Apr-2019].
[12] A. Shabani, *Thermal and radiochemical of neat and ATH filled EPDM : establishment of structure/properties relationships*. Paris, ENSAM, 2013.
[13] S.V. Suraci, D. Fabiani, S. Bulzaga, "About electrical and mechanical behaviour of low-voltage I&C cables used in nuclear power plants, "Modelling, measurement and control C", 2018, 79, pp. 79 – 82.
[14] S.V. Suraci, D. Fabiani, L. Mazzocchetti, V. Maceratesi, S. Merighi, "Investigation on Thermal Degradation Phenomena on Low Density Polyethylene (LDPE) through Dielectric Spectroscopy", IEEE Conference on Electrical Insulation and Dielectric Phenomena, CEIDP, 2018, pp. 434 – 437.
[15] J. Saunier, V. Mazel, C. Paris, and N. Yagoubi, "Polymorphism of Irganox 1076®: Discovery of new forms and direct characterization of the polymorphs on a medical device by Raman microspectroscopy," *European Journal of Pharmaceutics and Biopharmaceutics*, vol. 75, no. 3, pp. 443–450, Aug. 2010.